J|A|C|S
ARTICLES
Published on Web 03/13/2004

$Li_{17}Ag_3Sn_6$: A Polar Intermetallic π-System with Carbonate-like $[AgSn_3]^{11-}$ Anions and Trefoil Aromatic $[Ag_2Sn_3]^{6-}$ Layers

Corina Lupu,[†] Craig Downie,[†] Arnold M. Guloy,*[,†] Thomas A. Albright,*[,†] and Jiang-Gao Mao[‡]

Contribution from the Department of Chemistry and the Center for Materials Chemistry, University of Houston, Houston, Texas 77204-5003, and State Key Laboratory of Structural Chemistry, Fujian Institute of Research on the Structure of Matter, Chinese Academy of Sciences, Fuzhou 350002, People's Republic of China

Received October 3, 2003; E-mail: aguloy@uh.edu; talbright@uh.edu

Abstract: A new lithium silver stannide, $Li_{17}Ag_3Sn_6$, was synthesized from high-temperature reactions of the pure elements in tantalum containers. Its crystal structure, in the space group, $P31m$, with $a = 8.063(3)$ Å, $c = 8.509(4)$ Å, $Z = 1$, features two distinct AgSn-based anionic layers. Defect graphitic layers of Ag_2Sn_3, with ordered vacancies at one-third of the Ag sites, are alternately stacked with Kagome-like nets of isolated trigonal planar $AgSn_3$ units. Double layers of Li ions are sandwiched between the stacked AgSn-based layers. Theoretical calculations show unusual π-interactions within both anionic layers, with the trigonal planar $[AgSn_3]^{11-}$ units being isoelectronic with CO_3^{2-}. In addition, the chemical bonding of the layered $[Ag_2Sn_3]^{6-}$ π-network features incompletely filled lone-pair Sn states involved in in-plane trefoil aromatic interactions. Transport and magnetic susceptibility measurements on $Li_{17}Ag_3Sn_6$ indicate excellent metallic behavior and temperature-independent paramagnetism consistent with results from band structure calculations. The "trefoil" aromaticity, previously postulated for aromatic molecular systems, is finally observed, albeit in a polar intermetallic solid-state structure that lies at the border between metals and nonmetals.

Introduction

The Zintl concept has particularly proven to be an effective tool in rationalizing the structural properties and chemical bonding of materials along the border between metals and nonmetals.[1] In the spectrum from insulators to valence compounds to intermetallic compounds, we observe a continuous transition in their chemical bonding going from ionic to metallic. At the border between classical Zintl phases and normal metallic phases, typical properties of Zintl phases diminish and metallic conductivity appears. Thus, the smooth transition of chemical bonding and electronic properties from electron-precise to electron-deficient Zintl phases to nearly-free-electron intermetallic compounds provides a fertile area to search for materials with unique structural chemistry and novel electronic properties. The possibility of functional intermetallic materials is validated by several discoveries of polar intermetallics and Zintl phases that display complex combinations of structural, electronic, thermal, magnetic, and transport properties.[2−7] The novel discoveries include ternary and quaternary Zintl phases and polar intermetallics that exhibit high thermoelectric figures of merit,[3] giant magnetoresistances,[4] giant magnetocaloric effects,[5] mixed ionic-electronic conductivities,[6] and high-Tc superconductivity.[7]

Moreover, exploratory syntheses of complex intermetallic compounds along the Zintl border offer unique opportunities in refining the useful relationships between crystal structure, chemical bonding and physical properties. The structural peculiarities of Zintl phases are explained by assuming the presence of both ionic and covalent parts in the bonding picture.

[†] University of Houston.
[‡] Fujian Institute of Research on the Structure of Matter.

(1) (a) Corbett, J. D. *Angew. Chem., Int. Ed. Engl.* **2000**, *39*, 670. (b) Nesper, R. *Prog. Sol. St. Chem.* **1990**, *20*, 1. (c) Schaefer, H. *Ann. Rev. Mater. Sci.* **1985**, *15*, 1. (d) von Schnering, H. G.; Hönle, W. Chem. Rev. **1988**, *88*, 243.
(2) (a) He, T.; Huang, Q.; Ramirez, A. P.; Wang, Y.; Regan, K. A.; Rogado, N.; Hayward, M. A.; Haas, M. K.; Slusky, J. S.; Inumara, K.; Zandbergen, H. W.; Ong, N. P.; Cava, R. J. *Nature* **2001**, *411*, 54. (b) Pecharsky, V. K.; Gschneidner, K. A. *Adv. Mater.* **2001**, *13*, 683. (c) Guloy, A. M.; Goodey, *J. Condensed Matter News* **1998**, *7*, 1, 24−31.
(3) (a) Chung, D.-Y.; Hogan, T.; Brazis, P.; Rocci-Lane, M.; Kannerwurf, C.; Bastea, M.; Uher, C.; Kanatzidis, M. *Science* **2000**, *287*, 1024. (b) Sales, B. C.; Mandrus, D.' Williams, R. K. *Science* **1996**, *272*, 1325. (c) Iversen, B. B.; Palmqvist, A. E. C.; Cox, D. E.; Nolas, G. S.; Stucky, G. D.; Blake, N. P.; Metiu, H. *J. Solid St. Chem.* **2000**, *149*, 455. (d) Nolas, G. S.; Cohn, J. L.; Slack, G. A.; Schujman, S. B. *Appl. Phys. Lett.* **1998**, *73*, 178.
(4) (a) Chan, J. Y.; Kauzlarich, S. M.; Klavins, P.; Shelton, R. N.; Webb, D. J. *Chem. Mater.* **1997**, *9*, 3132. (b) Van Dover, R. B.; Gyorgy, E. M.; Cava, R. J.; Krajewski, J. J.; Felder, R. J.; Peck, W. F. *Phys. Rev. B* **1993**, *47*, 6134. (c) Baibich, M.; Broto, J.; Fert, A.; Nguyen van dau F.; Petroff, F. *Phys. Rev. Lett.* **1988**, *61*, 2472.
(5) (a) Pecharsky, V. K.; Gschneidner, K. A. *Phys. Rev. Lett.* **1997**, *78*, 4494. (b) Gschneidner, K. A.; Pecharsky, V. K. *Ann. Rev. Mater. Sci.* **2000**, *30*, 387. (c) Honda, K.; Hirone, T. *Nature* **1936**, *137*, 492.
(6) (a) Winter, M.; Besenhard, J. O. *Electrochim. Acta* **1999**, *45*, 31. (b) Weppner, W.; Huggins, R. A. *J. Solid State Chem.* **1977**, *22*, 297.
(7) (a) Nagamatsu, J.; Nakagawa, N.; Muranaka, T.; Zenitani, Y.; Akimitsu, J. *Nature* **2001**, *410*, 6824. (b) Campbell A. M. *Science* **2001**, *292*, 65. (c) Cava, R. J.; Takagi, H.; Batlogg, B.; Zandbergen, H. W.; Krajewski, J. J.; Peck., W. F.; van Dover: R. B.; Felder, R. J.; Siegrist, T.; Mizuhashi, K.; Lee, J. O.; Eisaki, H.; Carter, S. A.; Uchida, S. *Nature* **1994**, *367*, 146.

 10.1021/ja038868n CCC: $27.50

An electron transfer is formally assigned from the electropositive to the electronegative metals (polar part), resulting in anionic substructures that can be related to known isoelectronic covalent structures and molecules. A major criticism of the Zintl concept is the unreasonable assignment of ionic charges. However, the polar description of classical Zintl phases has been validated by accurate theoretical and experimental work, particularly if the assignment of the "charges" were in a formal oxidation sense.[8] Thus, the Zintl formalism actually represents the number of occupied Wannier-like electronic states of the polar intermetallic.[9] It is anticipated that metals (main group and transition metals and metalloids) with sufficient electronegativity differences will form what we term "polar intermetallics" wherein strong homo- and heterometallic bonding occurs within the covalent partial structure, and the valence generalities about Zintl phases still apply.

"Electron-Deficient" Polar Intermetallics

The validity (or lack thereof) of the classical Zintl formalism as applied to less polar intermetallics, involving metals along the Zintl border, is nicely probed by "electron-deficient" trelides. Seminal works by Corbett and Belin have established the propensity of polar intermetallic trelides (Ga, In, Tl) to form cluster-based anionic structures.[1a,10,11] The apparent "electron deficiency" in the chemical bonding of these cluster compounds is offset by the formation of three-center-two electron bonds, following the classic Wade-Mingos rules for boranes and expanded through isolobal analogies.[12] However, cluster-based intermetallic phases that do not obey even these rules have also appeared. These problems arose with extremely electron-deficient group 13 intermetallics that featured closed deltahedral frameworks but do not exhibit their canonical polyhedral form.[1a,10,13−17] Representative examples of these include $K_{10}Tl_7$,[14] K_8In_{11},[15] Sr_3Sn_5,[16] and $Na_8K_{23}Cd_{12}In_{48}$.[17] The unusual class of electron-deficient polar intermetallics is collectively known as hypoelectronic (yet electron-precise) systems. Molecular hypoelectronic analogues, such as metalloboranes of early transition metals, do exist and these exhibit accompanying geometrical irregularities.[18,19] In many of these cluster-based intermetallic compounds the cluster anions fulfill the electronic requirements for bonding albeit in the presence of excess electrons delocalized in a metal-based conduction band. The term "metallic Zintl phase" has been proposed to characterize the metallic hypoelectronic phases.[10] This characteristic is increasingly being recognized in describing many polar intermetallics that lie along the Zintl border.

A more unusual class of electron-deficient polar intermetallics are collectively known as "real" hypoelectronic systems with open valence bands, represented by compounds such as La_3In_4Ge, $SrIn_4$, and Sr_3In_5.[20−22] These constitute recent examples of truly hypoelectronic intermetallic systems with open and incompletely filled valence bands, having one- or two-electron deficiencies per formula unit. The unusual existence of an open valence band is responsible for the characteristic metallic behavior of real hypoelectronic systems. The remarkable stability of these hypoelectronic systems has been attributed to the significant role of cation sizes, as well as, matrix effects and Madelung contributions within the polar intermetallic structure.[21,22] The metallic hypoelectronic phases, including "metallic" Zintl phases, represent polar intermetallics that behave closest to the "nearly free electron" intermetallic compounds.

Intermetallic π-Systems

As in molecular chemistry, an alternative path to compensate for electron-deficiency is the formation of multiple bonds, through π-interactions, as in unsaturated and aromatic molecular systems. Our work probes the efficacy of the Zintl concept in rationalizing the stoichiometry, structure, and chemical bonding of complex electron-deficient Zintl phases exhibiting novel π-bonds. Their chemical bonding is reflected by their unusual crystal structures related to unsaturated hydrocarbons.[23] Several examples have been discovered, including the novel anionic zigzag chains, $[In{=}In{-}Ge]^{6-}$ in the semiconductor $SrCa_2In_2Ge$.[24] The anionic chains of the electron-deficient Zintl phase, with short In−In bonding distances, were characterized as being analogous and isoelectronic with an allyl anion chain $[CH{=}CH{-}CH_2]_\infty$.[15] Similarly, the $[Ga]^{2-}$ zigzag chains in CaGa have been likened to polyacetylene.[23a] Later, the polar intermetallic $Ca_5In_9Sn_6$ was discovered and found to exhibit an unprecedented intergrowth structure of Zintl and normal intermetallic layers.[25] More interestingly, the Zintl layers in $Ca_5In_9Sn_6$ feature isolated anionic $[In_3]^{5-}$ units that are isoelectronic with the aromatic cyclopropenium, $C_3H_3^+$. The $[In_3]^{5-}$ anions are also analogous to the $[Sn_3]^{2-}$ units in the superconducting $BaSn_3$.[26] In $Ca_5In_9Sn_6$, the valence states of the Zintl layers lie deep below the Fermi level, and the excellent metallic behavior of $Ca_5In_9Sn_6$ was attributed to the well-dispersed electronic states of the intermetallic layers that dominate the Fermi level.

Similar exploratory work by von Schnering and Nesper on ternary tetrelides (Si and Ge) resulted in the synthesis of arene-like π-systems, represented by $Ba_4Li_2Si_6$ and Li_8MgSi_6.[27,28] The novel lithium-based ternary $Ba_4Li_2Si_6$ features $[Si_6]^{10-}$ units

(8) (a) Seifert-Lorenz, K.; Hafner, J. *Phys. Rev B* **2002**, *66*, 94105. (b) Schmidt, P. C. *Struct. Bonding* **1987**, *65*, 91.
(9) (a) Nesper, R. *Angew. Chem., Int. Ed. Engl.* **1991**, *30*, 789. (b) Anderson, P. W. *Proc. Robert A. Welch Found. Conf. Chem. Res.* **1988**, *32*, 1. (c) Rudnik, J.; Stern, E. A. *Phys. Rev. B.* **1973**, *7*, 5062.
(10) (a) Corbett, J. D. In *Chemistry, Structure and Bonding of Zintl Phases and Ions*; Kauzlarich, S. M., Ed.; VCH Publishers: New York, 1996; p 139. (b) Corbett, J. D. *Inorg. Chem.* **2000**, *39*, 5178. (c) Corbett, J. D. *Struct. Bonding* **1997**, *87*, 157.
(11) Belin, C.; Tillard-Charbonnel, A. *Prog. Sol. St. Chem.* **1993**, *22*, 59.
(12) Wade, K. *Adv. Inorg. Chem. Radiochem.* **1976**, *18*, 1.
(13) Dong, Z. C.; Corbett, J. D. *J. Am. Chem. Soc.* **1993**, *115*, 11299.
(14) Kaskel, S.; Corbett, J. D. *Inorg. Chem.* **2000**, *39*, 778.
(15) Sevov, S. C.; Corbett, J. D. *Inorg. Chem.* **1991**, *30*, 4875.
(16) (a) Klem, M. T.; Vaughey, J. T.; Harp, J. G.; Corbett, J. D. *Inorg. Chem.* **2001**, *40*, 7020. (b) Zürcher, F.; Nesper, R.; Hoffmann, S.; Fässler, T. F. *Z. Anorg. Allg. Chem.* **2001**, *627*, 2211.
(17) Flot, D. M.; Tillard-Charbonnel, M.; Belin, C. H. E. *J. Am. Chem. Soc.* **1996**, *118*, 5229.
(18) Ghosh, S.; Beatty, A. M.; Fehlner, T. P. *J. Am. Chem. Soc.* **2001**, *123*, 9188.
(19) (a) King, R. B. *Inorg. Chem.* **2002**, *41*, 4722. (b) Wadepohl, H. *Angew. Chem., Int. Ed. Engl.* **2002**, *41*, 4220.
(20) Guloy, A. M.; Corbett, J. D. *Inorg. Chem.* **1996**, *35*, 2616
(21) Seo, D. K.; Corbett, J. D. *J. Am. Chem. Soc.* **2000**, *122*, 40, 1223.
(22) Seo, D. K.; Corbett, J. D. *J. Am. Chem. Soc.* **2001**, *123*, 19, 4512.
(23) (a) Miller, G. J. In *Chemistry, Structure and Bonding of Zintl Phases and Ions*; Kauzlarich, S. M., Ed.; VCH Publishers: New York, 1996; p 1. (b) Guloy, A. M.; Xu, Z.; Goodey, J. *ACS Symp. Ser.* **1999**, *727*, 2. (c) Eisenmann, B.; Cordier, G. In *Chemistry, Structure and Bonding of Zintl Phases and Ions*; Kauzlarich, S. M., Ed.; VCH Publishers: New York, 1996.
(24) Xu, Z.; Guloy, A. M. *J. Am. Chem. Soc.* **1998**, *120*, 42, 7349.
(25) Xu, Z.; Guloy, A. M. *J. Am. Chem. Soc.* **1997**, *119*, 10541.
(26) Fässler, T. F.; Kronseder, C. *Angew. Chem., Int. Ed. Engl.* **1997**, *36*, 2683.
(27) von Schnering, H. G.; Bolle, U.; Curda, J.; Peters, K.; Carillo-Cabrera, W.; Somer, M.; Schultheiss, W.; Wedig, U. *Angew. Chem., Int. Ed. Engl.* **1996**, *35*, 984.
(28) Nesper, R.; Curda, J.; von Schnering, H. G. *J. Solid State Chem.* **1986**, *62*, 199.

related to aromatic hydrocarbon rings such as benzene.[27] While quasiaromatic Si five-membered rings, $[Si_5]$,$^{6-}$ are featured in Li_8MgSi_6.[28] Moreover, condensed systems consisting of hexagonal Si_6 rings similar to arenes and conjugated polyaromatics have also been isolated and characterized.[29−34] The analogy of intermetallic to molecular π-systems also extends to organometallic systems. Recent work on alkaline earth metal nickel silicides has led to the discovery of Ba_2NiSi_3 − a novel polar transition metal intermetallic that features unprecedented metallocene-like $[NiSi_3]^{4-}$ chains.[35] Chemical bonding of the novel metallic chains were nicely rationalized as one-dimensional solid-state analogue of an extended metallocene.[36] The discovery of $Ba_4Li_2Si_6$, Ba_2NiSi_3 and other arene-like silicides strongly suggests the possibility of conceiving new posttransition and transition metal polar intermetallic systems displaying unusual structures and chemical bonding analogous to aromatic organic and organometallic molecules.[37] Moreover, the possibilities of novel electronic properties is emphasized by the variety of electronic behavior exhibited by polar intermetallic π-systems. These range from narrow gap semiconductors (e.g., $SrCa_2In_2Ge$) to excellent metals (e.g., $Ca_5In_9Sn_6$ and Ba_2NiSi_3), and even superconductors (e.g., $BaSn_3$ and MgB_2[7a]).

Late Transition Metal Polar Intermetallics

As in Zintl phases, intermetallic phases formed between late transition and posttransition metals with one or more of the electropositive alkali or alkaline earth metals often exhibit a variety of complex anionic structures.[23c,38] Formal charge transfer is anticipated to occur from the most electropositive metal to the covalent framework of late transition and/or posttransition metals. Several studies on transition metal polar intermetallics and compounds (e.g., borides, pnictides, and chalcogenides) have shown the effectiveness of the Zintl picture, in the framework of the rigid band, as a starting point in rationalizing crystal structures with respect to stoichiometry, chemical bonding, and properties.[1,9,23,39−44] The variety of structural anionic units (e.g., clusters, networks, and frameworks) in these compounds were observed to follow electronic valence rules consistent with the characteristic chemistry of the component elements. More interestingly, the various combinations of late transition metals with post-transition metals also provide interesting chemical solid-state systems wherein interplay of electronic and magnetic effects can be investigated.

Early studies by Schäffer on the chemistry of polar intermetallics of the alkali metals with late transition metals and post-transition metals of groups 14 and 15 revealed a wealth of anionic structural motifs.[1c,45−48] Different anionic arrangements, including linear trinuclear units (e.g., $(Sb-Cu-Sb)^{5-}$ in K_5CuSb_2),[45] zigzag chains (e.g., $[AgSb]^{2-}$ and $[AgBi]^{2-}$ in Na_2AgSb and K_2AgBi, respectively),[46] and corrugated hexagonal nets (e.g., $[Ag_3As_2]^{3-}$ in $K_3Ag_3As_2$),[47] were discovered. Similar alkaline earth metal phases such as SrZnGe and CaCuSi, with anionic hexagonal nets (AlB_2-structure type), have also been prepared.[48] Moreover, chemical bonding of the complex late-transition metal polar intermetallics were successfully rationalized using the extended-Zintl concept.[23a,9a,49−50] However, just how far to the left of the Zintl border would the effective charge transfer from the electropositive metals to the electronegative metal partners persist is yet to be determined.

The chemistry of Li-rich intermetallic phases often show complex compositions and unique structures, different from the rest of the alkali metals.[1b,51,52] The higher electron affinity, smaller size and stronger polarizing ability of Li allows for the stabilization of anionic substructures with higher formal charges. Moreover, the bonding picture of Li-based polar intermetallics Li−X (X = post-transition metals) with Li-poorer Li/X ratios usually adheres to the Zintl rule. While polar intermetallics with higher Li:X ratios do not necessarily conform to the Zintl concept. The "excess" charges in Li-rich polar intermetallics has been attributed to the formation of Li-based "cage orbitals".[52] Results of a recent structural and physical study on $Li_{17}Sn_4$ − the most Li-rich phase in the Li−Sn system − pose more questions regarding the validity of the classical Zintl picture.[53] Our investigations on lithium/late transition metal/post-transition metal polar intermetallics is also motivated by the possibility of discovering layered intermetallic systems that exhibit unusual chemical bonding and exotic transport properties (e.g., superconductivity and mixed ionic-electronic conductivity). Herein we report on the synthesis, crystal structure, chemical bonding, and properties of a novel layered polar intermetallic, $Li_{17}Ag_3Sn_6$.

Experimental Section

Synthesis. The air-sensitive brittle gray compound, $Li_{17}Ag_3Sn_6$, was obtained as crystals from the reaction of nearly stoichiometric amounts of the pure elements: lithium foil (99.99%, Aldrich), silver shots (99.99%, Aldrich), and tin shots (99.999%, Alfa Aesar), in welded Ta tubes within an evacuated quartz jacket. A slight excess (~12%) of lithium and (12%) silver was necessary in order to obtain sufficiently sized single crystals. All sample manipulations were performed in a purified argon atmosphere glovebox, with a moisture level <0.01 ppm. The reaction mixture was first heated to 250 °C, at a rate of 0.2 °C/min, to melt Li and Sn. Subsequently, the temperature was slowly increased to 850 °C and held at that temperature for 24 h. The reaction was slowly cooled over 33 h to 650 °C and annealed for 5 days. Finally, the reaction was slowly cooled to 100 °C, over 3 days, and brittle dark gray crystals of the title compound were obtained. Annealing at 650

(29) Müller, W.; Schaefer, H.; Weiss, A. *Z. Naturforsch. B* **1970**, *25*, 1371−1374.
(30) Nesper, R.; Currao, A.; Wengert, S. *Chem. Eur. J.* **1998**, *4*, 2251.
(31) Currao, A.; Wengert, S.; Nesper, R.; Curda, J.; Hillebrecht, H. *Z. Anorg. Allg. Chem.* **1996**, *622*, 501.
(32) Currao, A.; Nesper, R. *Angew. Chem., Int. Ed. Engl.* **1998**, *37*, 841.
(33) Wengert, S.; Nesper, R. *Inorg. Chem.* **2000**, *39*, 2861.
(34) Wörle, M.; Nesper, R. *Angew. Chem., Int. Ed. Engl.* **2000**, *39*, 2349.
(35) Goodey, J.; Mao, J.; Guloy, A. M. *J. Am. Chem. Soc.* **2000**, *122*, 10478−10479.
(36) Lichtenberger, D. L.; Hoppe, M. L.; Subramanian, L.; Kober, E. M.; Hughes, R. P.; Hubbard, J. L.; Tucker, D. S. *Organometallics* **1993**, *12*, 2025.
(37) Goodey, J. Ph.D. Dissertation, University of Houston, Houston, 2001.
(38) von Schnering, H. G.; Nesper, R.; Curda, J.; Tebbe, K. F. *Angew. Chem., Int. Ed. Engl.* **1980**, *19*, 1033.
(39) Liebman, J. F.; Vincent, J. S. *Angew. Chem., Int. Ed. Engl.* **1982**, *21*, 632.
(40) Kauzlarich, S. M. *Comm. Inorg. Chem.* **1990**, *10*, 2&3, 75−88.
(41) von Schnering, H. G. *Angew. Chem., Int. Ed. Engl.* **1981**, *20*, 33.
(42) Savelsberg, G.; Schäfer, H. *Z. Naturforsch.* **1979**, *34b*, 771−773.
(43) Schuster, H. U.; Mues, C.; Jung, W. *Z. Naturforsch.* **1978**, *34b*, 354−355.
(44) Rieger, W.; Parthé, E. *Monatsch. Chem.* **1969**, *100*, 439.
(45) Savelsberg, G.; Schäfer, H. *Z. Naturforsch.* **1977**, *32b*, 745−748.
(46) Savelsberg, G.; Schäfer, H. *Z. Naturforsch.* **1979**, *34b*, 1033.
(47) Dörrscheidt, W.; Niess, N.; Schäfer, H. *Z. Naturforsch.* **1977**, *32b*, 985.
(48) Schäfer, H.; Eisenmann, B.; May, N.; Müller, W. *Angew. Chem., Int. Ed. Engl.* **1973**, *12*, 9 694−712.
(49) (a) Haussermann, U.; Svensson, C.; Lidin, S. *J. Am. Chem. Soc.* **1998**, *120*, 3867. (b) Nordell, K. J.; Miller, G. J. *Inorg. Chem.* **1999**, *38*, 579.
(50) Drews-Nicolai, L.; Hohlneicher, G.; Hoppe, U.; Jung, W. *Z. Anorg. Allg. Chem.* **2001**, *627*, 1157.
(51) Nesper R.; von Schnering H. G., Curda J. *Chem . Ber.* **1986**, *119*, 3576.
(52) Ramirez, R.; Nesper, R.; von Schnering, H. G., Böhm, M. *J. Phys. Chem.* **1987**, *48*, 51.
(53) Lupu, C.; Mao, J.-G.; Rabalais, J. W.; Guloy, A. M.; Richardson, J. W., Jr. *Inorg. Chem.* **2003**, *42*, 3765.

°C was necessary to obtain high reaction yields (~90%). However, a pure crystalline phase cannot be obtained even when the reactions were quenched. An unknown minor phase (~10%) was observed, based on four diffraction peaks, that could not be indexed to any known binary or ternary phase in the Li−Ag−Sn system. The observed thermal behavior of the reaction and the inability to obtain pure phase products suggest that the compound, $Li_{17}Ag_3Sn_6$, is peritectic and melts incongruently.

Crystallography. Crystal structure investigations were performed on powder and single crystals by X-ray diffraction. Dark gray single crystals were isolated and chosen from the bulk phase, within a glovebox equipped with a microscope, transported under Ar atmosphere to a Siemens SMART diffractometer equipped with a 1K CCD area detector. The crystals were mounted on the goniometer attached to the diffractometer, under a −50 °C N_2 flow. Data were collected using a Mo Kα X-ray source (λ = 0.71073 Å).

The cell constants were indexed from 35 reflections chosen from 60 frames collected with 15 s exposure per frame. A hemisphere of data (1271 frames at 5 cm detector distance) was collected by narrow-frame method with scan widths of 0.3° in ω and exposure time of 40 s per frame, up to $2\theta_{max}$= 56.06°. The first 50 frames were recollected at the end of data collection to assess the stability of the crystal, and the decay in intensities was found to be less than 1.0%. A total of 2972 reflections were measured, of which 801 reflections were unique and 690 reflections with $I > 2\sigma_I$ were considered observed. Data were corrected for Lorentz factors, polarization and air absorption due to variations in the path length through the detector faceplate. Empirical absorption correction was applied using the SADABS program.[54,55] The Laue class was −31m, based on the data averaging and R_{int} values, and the possible space groups were *P*312, *P*31*m*, and *P*-31m. The space group *P*31*m* was found to be correct, based on the successful results of the structural refinement. The phase problem was solved by direct methods (SHELXTL)[54,55] revealed all the Ag and Sn positions. The Li positions were subsequently located from careful analyses of difference Fourier maps.

Initial refinements in space groups *P*312 and *P*-31m resulted in the composition $Li_{18}Ag_3Sn_6$ ($R1 > 6.0\%$), but these refinements exhibited convergence problems. Moreover, one Li position was later found to exhibit an abnormally large U_{eq} (~0.55 Å^2), which was at least 20 times larger than those of the remaining Li atoms. The problematic position was removed and the rest of the Li positions were refined isotropically in space group *P*31*m*. Least squares refinement in space group *P*31*m* of the atomic coordinates, anisotropic thermal parameters for Ag and Sn, and isotropic parameters for Li (37 variables; S = 1.16, R1 = 0.0446, and wR2 = 0.0977 for observed data) successfully converged to a composition of $Li_{17}Ag_3Sn_6$. Being too light compared to Ag and Sn, all Li atoms were treated like hydrogen atoms in coordination compounds and assigned reasonable average thermal parameters (0.02 Å^2). The additional constraints slightly increased the R1 values (5.1%). However, validation of this approach was previously provided by neutron and X-ray diffraction studies on $Li_{4.4}Sn$.[53] Herein, we report results of refinements on $Li_{17}Ag_3Sn_6$ with fixed Li thermal parameters (Ueq). A summary of the relevant crystallographic data is presented in Table 1. List of atomic parameters, along with the relevant bond distances and angles are presented in Tables 2 and 3, respectively.

On the basis of the crystal structure refinement, there are no partial or mixed occupancies at the Ag and Sn positions. Final difference Fourier maps were essentially featureless with residual peaks (±1.8 e/Å^3) that are all within 0.4 Å from Sn(2). Chemical compositions of a number of single crystals were also analyzed by WDS (wavelength dispersive spectrometer). Results indicate an atomic ratio of 2:1 for Sn:Ag, in good agreement with the refinement results. Since an accurate analysis for Li by X-rays is difficult, lithium composition was indirectly confirmed by the high yield (90%) synthesis of the compound with nominal composition, and the nearly invariant lattice constants with Li composition. Accurate lattice constants were obtained by careful indexing of X-ray diffraction patterns, with NBS Si as an internal standard, to the theoretical pattern calculated from the results of single-crystal refinement. Chemical analysis on a bulk sample also confirmed the Ag:Sn stoichiometry obtained from the single-crystal refinement.

Table 1. Summary of Crystal Data, Intensity Measurements, and Structure Refinement for $Li_{17}Ag_3Sn_6$

formula weight (g/mol)	1153.73
crystal size (mm)	0.06 × 0.06 × 0.02
T (K)	223(2)
wavelength, Mo Kα(Å)	0.71073
space group	*P*31*m* (157)
a (Å)	8.063(3)
C (Å)	8.510(4)
V (Å^3)	479.1(4)
Z	1
d_{calc} (g/cm^3)	3.999
μ (mm^{-1})	10.640
2θ range (deg)	2.39−28.03
index ranges	$-10 \le h \le 9$
	$-10 \le k \le 8$
	$-9 \le l \le 11$
reflections collected	2972
independent reflections	801
R^a indices ($I > 2\sigma$)	$R_1 = 0.045$, w$R_2 = 0.098$
R^a indices (all data)	$R_1 = 0.051$, w$R_2 = 0.102$
max. peak and hole (e/Å^3)	−1.784 and 1.800

[a] $R_1 = \sum||F_o| - |F_c||/\sum|F_o|$; w$R_2 = [\sum w(|F_o|^2 - |F_c|^2)^2/\sum w(|F_o|^2)^2]^{1/2}$, $w = 1/(\sigma_F^2)^2$.

Table 2. Atomic Coordinates [Å] and Equivalent Isotropic Thermal Parameters [Å^2] for $Li_{17}Ag_3Sn_6$

atom	x	y	z	U_{iso}
Sn1	0.3482(2)	0.3482(2)	0.4993(1)	0.009(1)
Sn2	0	0.3158(2)	0.0013(2)	0.010(1)
Ag3	0	0	0.5066(3)	0.014(1)
Ag4	0.3333	0.6667	0.0059(2)	0.012(1)
Li1	0.356(4)	0.356(4)	0.144(4)	0.02
Li2	0	0.304(4)	0.326(4)	0.02
Li3	0.307(4)	0	0.651(4)	0.02
Li4	0.358(4)	0.358(4)	0.815(4)	0.02
Li5	0.3333	0.6667	0.678(4)	0.02
Li6	0.6667	0.3333	0.343(4)	0.02
Li7	0	0	0.868(4)	0.02

Table 3. Relevant Interatomic Distances (Å) and Angles (deg) for $Li_{17}Ag_3Sn_6$

Ag1−Sn1 = 4.925 (15)	Sn2−Ag1−Sn2 = 119.96(10)
Ag1−Sn2 = 2.807 (16)	Ag3−Sn1−Ag3 = 114.83(5)
Ag2−Sn1 = 2.763 (12)	Sn1−Ag3−Sn1 = 119.96(4)
Ag2−Sn2 = 5.047 (16)	
Ag3−Sn1 = 2.762 (10)	
Sn2−Sn2 = 4.554 (16)	

Properties. The electronic transport behavior of the air-sensitive material, $Li_{17}Ag_3Sn_6$, was determined by the electrodeless "Q" method,[56,57] with the aid of a Hewlett-Packard 4342A Q Meter. Selected powder samples (98 mg) were sieved to 250−425 μm, diluted with chromatographic Al_2O_3, and sealed under He in a Pyrex tube. The Q-measurements were made at 34 MHz over the temperature range from 100 to 280 K. Magnetic susceptibility measurements (zero-field cooled and field-cooled) were carried out at under varying applied fields (up

(54) Sheldrick, G. *SHELXL96*; Institut fuer Anorganische Chemie: Göettingen, Germany, 1996.
(55) Sheldrick, G. M. *Programs for Crystal Structure Analysis (Release 97−2)*: Institut für Anorganische Chemie der Universität: Göttingen, Germany, 1998.
(56) El-Hanany, U. *Rev. Sci. Instrum.* **1973**, *44*, 8, 1067.
(57) Shinar, J.; Dehner, B.; Beaundry, B. J.; Peterson, D. T. *Phys. Rev. B* **1988**, *37*, 4, 2066.

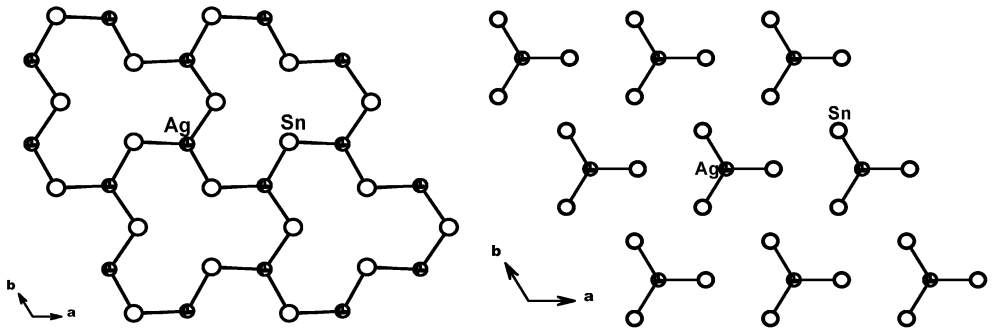

(a) *(b)*

Figure 1. (a) The structure of a $[Ag_2Sn_3]^{6-}$ layer (Sn atoms, white circles; Ag atoms, octant-shaded circles); (b) the structure of a $[AgSn_3]^{11-}$ layer (Sn atoms, white circles; Ag atoms, octant-shaded circles).

Table 4. Atomic Parameters Used for Extended Hückel Calculations on $Li_{17}Ag_3Sn_6$[a]

atom type	orbital	H_{ii} (eV)	ξ_1	ξ_2	C_1[b]	C_2[b]
Sn	s	−16.16	2.12	1.00		
	p	−8.32	1.82	1.00		
Ag	s	−9.24	2.10	0.5436	1.100	0.5751
	p	−3.54	1.49	1.00	0.000	0.0000
	d	−13.23	4.05	0.5798	1.800	0.5756
B	s	−15.2	1.3		1.000	
	p	−8.5	1.3		1.000	
N	s	−26.0	1.95		1.000	
	p	−13.4	1.95		1.000	

[a] H_{ii} values are the diagonal matrix elements $\langle\lambda_1|H^{eff}|\lambda_1\rangle$, where H^{eff} is the effective Hamiltonian. In our calculations of the off-diagonal matrix elements $H^{eff} = \langle\lambda_1|H^{eff}|\lambda_1\rangle$, the weighted formula was used. [b] Contraction coefficients used in the double-ζ Slater-type orbital.

to 0.01 T) over a temperature range of 4−295 K. The measurements were performed on a pressed pellet sample (0.075 g), using a Maglab 9T vibrating sample magnetometer (VSM) from Oxford Instruments.

Extended Hückel Band Calculations. Electronic structure tight binding calculations were performed using the extended Hückel method in order to correlate structure−property relationships and to obtain information regarding the nature of the bonding of $Li_{17}Ag_3Sn_6$.[58,59] The band structure calculations along with the Density of States (DOS) and Crystal Orbital Overlap Population (COOP) curves were performed using the Crystal And Electronic Structure Analyzer (CAESAR) software package and the revised BIGBAND software.[60] The atomic parameters used in the calculations along with the H_{ii} and Slater exponents are presented in Table 4. Double-ζ expansions were used for the d orbitals of silver.

Results and Discussion

The ternary Li−Ag−Sn system, particularly the Li-richer phases, has not been extensively investigated. So far, there have been only two ternary Li−Ag−Sn phases reported, namely, Li_2AgSn and $LiAg_2Sn$.[61,62]

Both Li_2AgSn and $LiAg_2Sn$ were found to crystallize in salt-like closed packed structures that are related to the well-known NaTl and NaCl structure types, respectively. Also, both binaries represent the Li-poorer side of the phase diagram. The anionic $[AgSn]^{2-}$ framework in Li_2AgSn is a diamond network, with each Sn atom tetrahedrally coordinated by Ag atoms and vice versa.[61] In $LiAg_2Sn$, the 3D ionic framework features cubic closed packed arrangement of Sn atoms, wherein the atoms are at the corners and the face-centers of the cubic cell (as in the Cl positions).[62] The Li atoms occupy the octahedral sites (Na in NaCl), represented as the center of the cubic edges (Na positions). The Ag atoms are located at the tetrahedral interstices of the cubic closed packed Sn arrangement. The synthesis of $Li_{17}Ag_3Sn_6$ represents a new structure type in the chemistry of intermetallics, and is the first example of a Li−Ag−Sn phase having a layered anionic structure.

Structural Description. The title compound, crystallizes in the trigonal space group, $P31m$, with $a = 8.063(3)$ Å, $c = 8.510(4)$ Å, $Z = 1$. The crystal structure can be described as alternate stacking of two types of Ag−Sn anion layers, namely, a defect graphitic Ag_2Sn_3 network and a nominal filled-Kagome $AgSn_3$ layer. The lithium atoms form double cationic layers intercalated between the stacked anionic sheets.

The first anionic layer, $_{2D}[Ag_2Sn_3]$, can be derived from an ordered-defect heteroatomic 6^3 graphitic net as in $_\infty^2$(BN). The ordered vacancy occurs at one-third of the Ag sites in ideal AgSn graphite net and results in the formation of a layered net composed of fused 12-membered rings (see Figure 1a). The 12-membered Ag_6Sn_6 rings are analogous to a hetero[12]annulene unit.[63] Each Ag atom in the $_{2D}[Ag_2Sn_3]$ layer is coordinated to three Sn atoms and has a trigonal planar geometry (Sn2−Ag1−Sn2 = 119.96°(4)). Each Sn atom is coordinated to two Ag atoms with Ag−Sn−Ag bond angles of 114.83°(5). The Ag−Sn bond distance in the $_{2D}[Ag_2Sn_3]$ layer, of 2.761(12) Å, is shorter than the Ag−Sn distances in Li_2AgSn and $LiAg_2Sn$ (2.837 and 2.854 Å, respectively), but comparable to the bonding distances (2.77 Å) in the graphitic AgSn layered network in YbAgSn.[64] The nearest neighboring distances between Sn atoms − across the defect site − in the $_{2D}[Ag_2Sn_3]$ layer is 4.410 Å. A similar ordered-defect graphite anion network has been reported for Yb_3Si_5, where the analogous Si_5 layered structure was characterized as being an $[Si_5]^{8-}$ anion that satisfies the $8 - N$ rule.[65,66] However, the minor structural differences between the $[Si_5]^{8-}$ layers of Yb_3Si_5 and the $_{2D}[Ag_2Sn_3]$ layer in $Li_{17}Ag_3Sn_6$ have significant effects on their chemical bonding and electronic description, and will be further discussed below.

(58) Hoffmann, R. *J. Chem. Phys.* **1963**, *39*, 1397.
(59) Whangbo, M.-H.; Hoffmann, R. *J. Am. Chem. Soc.* **1978**, *100*, 6093.
(60) Whangbo, M. H.; Ren, J.; Weigen, L. *CAESAR*; North Carolina State University: Raleigh, 1998.
(61) Pauly, H.; Weiss, A.; Witte, H. *Z. Metallkde.* **1968**, *59*, 47.
(62) Schuster, H. U.; Thiedemann, D.; Schoenemann, H. *Z. Anorg. Allg. Chem.* **1969**, *370*, 160.
(63) Oth, J. F. M.; Röttele, H.; Schröder, G. *Tetrahedron Lett.* **1970**, 61.
(64) Pöttgen R.; Wu Z.; Hoffmann R.; Kuβmann D. *Z. Anorg. Allg. Chem.* **1998**, *624*, 945.
(65) Iandelli, A.; Palenzona, A.; Olcese, G. L. *J. Less-Common Met.* **1979**, *64*, 213.
(66) Pöttgen R.; Arpe P. E.; Felser C.; Kuβmann D.; Müllmann R.; Mosel B. D.; Künnen B.; Kotzyba G. *J. Solid State Chem.* **1999**, *145*, 668.

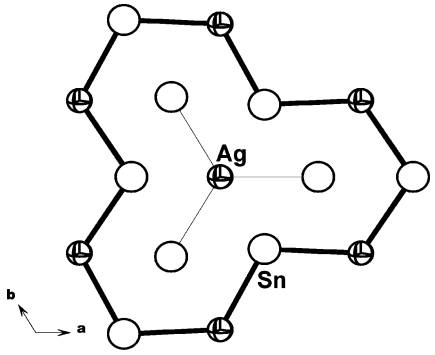

Figure 2. The stacking arrangement of the $[Ag_2Sn_3]$ layers and $[AgSn_3]$ units as viewed down the *c*-axis (Sn atoms, white circles; Ag atoms, octant-shaded circles).

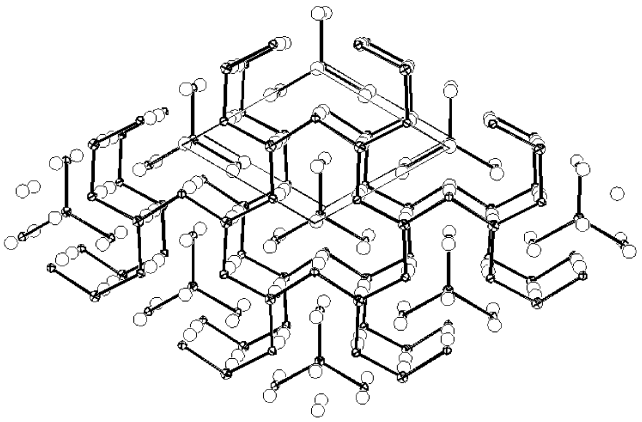

Figure 3. ORTEP representation of the crystal structure of $Li_{17}Ag_3Sn_6$ (Sn atoms, crossed ellipsoids; Ag atoms, octant-shaded ellipsoids; Li atoms, isotropic ellipsoids). The hexagonal unit cell is outlined.

The second anionic layer in $Li_{17}Ag_3Sn_6$ can be considered as being comprised by isolated trigonal planar $AgSn_3$ fragments (see Figure 1b). The trigonal planar $[AgSn_3]$ units are derived from a Kagome net of Sn atoms, with Ag atoms occupying the centers of one-third of the Kagome net's Sn_3 triangles. The resulting formation of $AgSn_3$ filled-Kagome nets result in Ag−Sn distances of 2.808(6) Å and Sn−Ag−Sn angles of 119.96°-(10). The Ag−Sn distances in the $AgSn_3$ fragments are longer than those observed in the $_{2D}[Ag_2Sn_3]$ network but still shorter than those observed for Li_2AgSn and $LiAg_2Sn$. Moreover, the relative contraction of the Sn_3 triangles around the Ag centers results in a distortion from the ideal Sn Kagome net, with inequivalent Sn−Sn intra- and intermolecular distances of 4.862 and 4.555 Å, respectively.

Equivalent trigonal planar AX_3 anion units have been previously reported in Zintl phases formed by alkali metals (A), tetrels (T) and pnictogens (P), A_5TP_3, as in $Cs_5(SiP_3)$.[67] The ternary tetrelide pnictides, $A_5(TP_3)$, contain trigonal prisms of A (Cs, and Rb) atoms that are centered by trigonal planar units of $[TP_3]^{5-}$ (T = Si−Sn; P = P, As). Following the Zintl picture, the 24-electron $[TP_3]^{5-}$ trigonal planar units are therefore analogous to the $[CO_3]^{2-}$ anion.

The two anionic layers, $_{2D}[Ag_2Sn_3]$ and $AgSn_3$, are alternately stacked along the *c*-axis in a manner where the Ag atoms of the $AgSn_3$ units of the second layer lie directly above and below the vacant Ag-sites of the $_{2D}[Ag_2Sn_3]$ layer. Thus, a projection of the two anionic layers, along the *c*-axis, on the *a*−*b* plane show the 12-membered Ag_6Sn_6 rings of the $_{2D}[Ag_2Sn_3]$ layer closely envelop the $AgSn_3$ units, as shown in Figure 2.

The stacking sequence of the anion layers and the Li layers is as follows: $[AgSn_3]$, [Li], [Li], $[Ag_2Sn_3]$, [Li], [Li]. Double layers of lithium atoms effectively separate and isolate the anionic layers in $Li_{17}Ag_3Sn_6$, and the closest interlayer distance between two adjacent anionic layers is ∼5.046 Å. The crystal structure for the title compound is illustrated in Figure 3.

The layers of lithium atoms adjacent to the $_{2D}[Ag_2Sn_3]$ layers form Li_6 trigonal prisms around the Ag atoms (see Figure 4a). The height of the Li_6 prisms is 2.786(14) Å, and the nearest Li−Li distances, along the prism triangles, are 4.507(10) Å. The nearest neighboring Li−Sn and Li−Ag interatomic distances relevant to the Li_6 trigonal prisms are 2.970(19) and 2.845(3) Å, respectively. A trigonal pyramidal Li_2Sn_3 environment is formed around the vacant sites of the $_{2D}[Ag_2Sn_3]$ network, with the three Sn atoms as a triangular base (equatorial) and two Li atoms (axial) directly above and below the vacancy. The Li−Sn (axial−equatorial) distance in the nominal Li_2Sn_3 trigonal bipyramid is 2.788(4) Å.

Similar arrangements of Li atoms are observed for the second anionic $[AgSn_3]$ layer (see Figure 4b). The Ag atoms of the $[AgSn_3]$ layers lie at the center of Li_6 trigonal prisms that have prism heights of 2.784(14) Å, and a Li−Li triangular distance of 4.851 Å. The resulting Li−Sn and Li−Ag bonds are 2.999-

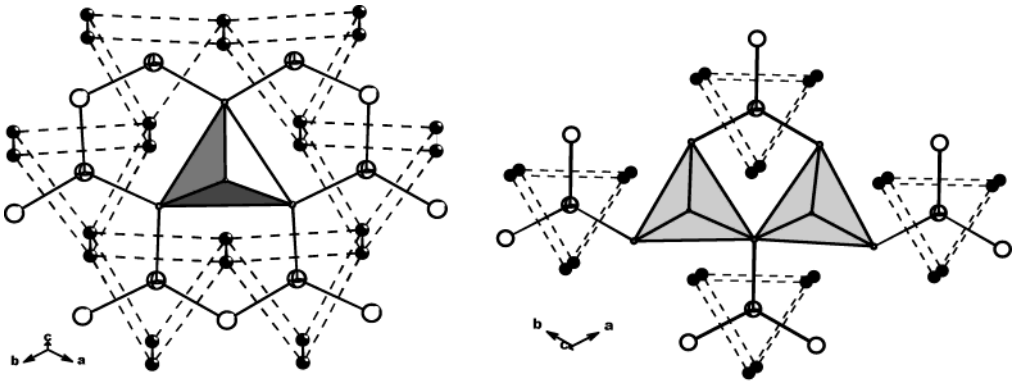

Figure 4. (a) The arrangement of the Li atoms corresponding to the $[Ag_2Sn_3]$ layer (Sn atoms, white circles; Ag atoms, octand-shaded circles; Li atoms, black circles); (b) the arrangement of the Li atoms corresponding to the $[AgSn_3]$ layer (Sn atoms, white circles; Ag atoms, octand-shaded circles; Li atoms, black circles).

(3) Å and 2.828(4) Å, respectively. The adjacent $AgSn_3$ units are linked through Li atoms that form nominal trigonal bipyramidal units with the terminal Sn atoms of three neighboring $AgSn_3$ fragments.

On the basis of the electronegativity differences and application of the polar Zintl scheme, a complete charge transfer from lithium to the [AgSn] networks may be assumed. Thus, the electron allocation can be approximated as $Li_{17}[\{AgSn_3\}^{-x}\{Ag_2Sn_3\}^{-y}]$ with $(x + y = 17)$. Furthermore, we can assume that the isolated trigonal planar $AgSn_3$ units are isoelectronic with the 24-electron anions, $[CO_3]^{2-}$ and $[SiP_3]^{5-}$, and formulated as $[AgSn_3]$.[11−68]

The assumption that the Ag_2Sn_3 defect-graphite layer would follow the $8 - N$ rule leads to the assignment as an $[Ag_2Sn_3]^{14-}$ anion. The $[Ag_2Sn_3]^{14-}$ assignment is based on the formal coordination (2-center-2electron bonds) of the (3-bonded) Ag and the (2-bonded) Sn atoms. Thus, the simple Zintl $(8 - N)$ scheme for $Li_{17}Ag_3Sn_6$, as $[AgSn_3]^{11-} + [Ag_2Sn_3]^{14-} \neq -17$ (from 17 Li+), is not valid. This indicates that $Li_{17}Ag_3Sn_6$ is significantly electron-deficient. To understand and rationalize the perceived electron deficiency in the chemical bonding of the complex lithium silver stannide, theoretical band structure calculations and electronic transport and magnetic susceptibility measurements were performed.

Electronic Structure and Chemical Bonding. Tight binding calculations with an extended-Hückel Hamiltonian were carried out to investigate the chemical bonding description in $Li_{17}Ag_3Sn_6$. A rigid band approach was initially performed, wherein the lithium atoms were neglected, calculating the electronic structure based only on the anionic network composed of Ag and Sn atoms.[68] There are then two layers: one composed of the isolated trigonal planar units $[AgSn_3]$, and the other that is composed of a two- dimensional slab composed of $[Ag_2Sn_3]$ units. The layers are well separated from each other (>5 Å) so each can be separately investigated.

With a trigonal planar geometry the $[AgSn_3]$ units are assigned to be isoelectronic with the 24 valence electron molecules $[CO_3^{2-}]$, $[BF_3]$, and $[(SiP_3)^{5-}]$. Thus, the Ag and three Sn atoms contribute a total of 13 electrons that results in the formal assignment of $[AgSn_3]^{11-}$ for an isoelectronic trigonal planar unit. Band structure and DOS calculations carried out on the $[AgSn_3]^{11-}$ layers show very small dispersions, consistent with the molecular nature of the $[AgSn_3]^{11-}$ fragments. Moreover, a large band gap (Eg = 4.4 eV) is observed from the calculations. Therefore, since there are ten Li atoms associated with this layer, the electron count for the Li−$AgSn_3$−Li slab is $[Li^+_{10}(AgSn_3)^{11-}]$. In other words the Li−$AgSn_3$−Li sandwich has a net negative charge of 1 per formula unit.

Given an electronic count of $[AgSn_3]^{11-}$ for the first layer, the second sandwich layer Li−Ag_2Sn_3−Li must be assigned as $Li_7^+[Ag_2Sn_3]^{-6}$. The density of states (DOS) and the crystal overlap population (COOP) for Ag−Sn interactions, resulting from two-dimensional band structure calculations on a $[Ag_2Sn_3]^{-6}$ layered network, are presented in Figure 5. The Sn p_x and p_y contribution to the DOS is given by the dashed line, where the x and y axis correspond to the Ag−Sn coordination plane. The region below −11 eV corresponds primarily to the Ag 4d states.

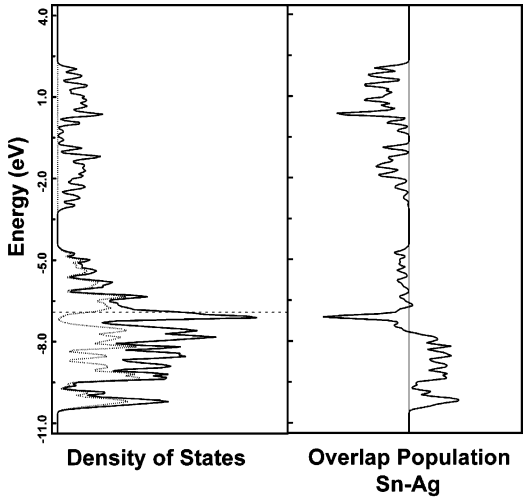

Figure 5. Plots of the DOS (total DOS, solid line; projections of Sn p_x and p_y contributions, dotted line) and COOP (Ag−Sn interactions) in the $[Ag_2Sn_3]$ net. The Fermi level for $[Ag_2Sn_3]^{6-}$ is given by a dashed line.

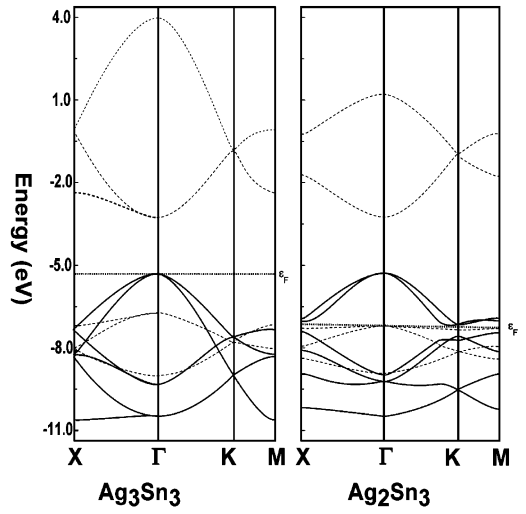

Figure 6. Band dispersions of a hypothetical $[Ag_3Sn_3]^{9-}$ with the BN structure (left) and the defect-graphite $[Ag_2Sn_3]^{6-}$ (right) (σ-bands, filled line; π-bands, dashed line). The labels, **X**, **Γ**, **K**, and **M** correspond to (π/a, 0), (0, 0), (π/a, π/a), and (0, π/a), respectively.

Those above the Fermi level, from ∼ −3.0 to −2.5 eV are primarily unoccupied π^* levels which are Ag−Sn antibonding in character and have greater contributions from the more electropositive Ag atoms. The more important electronic states around the Fermi level are primarily Ag and Sn σ and π levels. As indicated by the Sn p_x/p_y projection in the DOS, the σ levels, localized almost exclusively on Sn, lie just below the Fermi level to ∼ −4 eV. The large peak just below the Fermi level is the π band primarily derived from Ag and Sn out-of-plane p_z orbitals. As will be discussed shortly, this π band surprisingly exhibits very small dispersion across the Brillouin zone. Moreover, as evidenced by the COOP plot, these π states have Ag−Sn antibonding character.

The electronic band structure of $[Ag_2Sn_3]^{-6}$, around the Fermi level, is presented at the right-hand side of Figure 6. Solid and dashed lines indicate the relevant bands with σ and π symmetries, respectively. Within the coordinate system provided in **1**, the two degenerate π bands just below the Fermi level are drawn in **2** and **3** at the Γ point, $(\mathbf{k}_x = \mathbf{k}_y = 0)$. Topologically they are derived from the two highest filled π levels of a

(67) Eisemann, B.; Klein, J.; Somer, M. *Angew. Chem., Int. Ed. Engl.* **1990**, *29*, 87.
(68) Albright T. A.; Burdett J. K.; Whangbo M. H. *Orbital Interactions in Chemistry*: Wiley: New York, 1985.

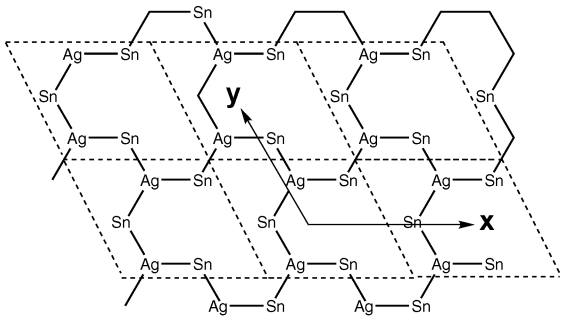

1

pentadienyl unit except that in each case there is significant antibonding between the p_z AO's on Sn and d orbitals at Ag. One member of the degenerate pair remains Ag−Sn antibonding upon going from Γ ($\mathbf{k}_x = \mathbf{k}_y = 0$) to **K** ($\mathbf{k}_x = \mathbf{k}_y = \pi/\mathbf{a}$); see **4**. Hence, this band is nearly flat throughout the Brillouin zone. On the other hand, crystal orbital **3** loses Sn p_z−Ag d antibonding at the **K** point and in fact becomes somewhat Sn p_z−Ag p_z bonding, see **5**. Therefore, **3** is stabilized to lower energies on going to the **K** point.

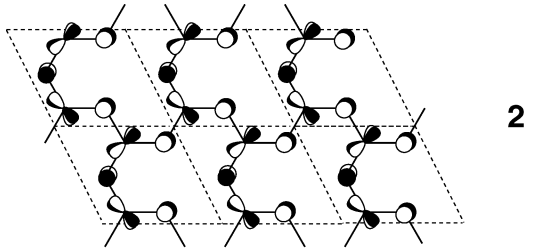

2

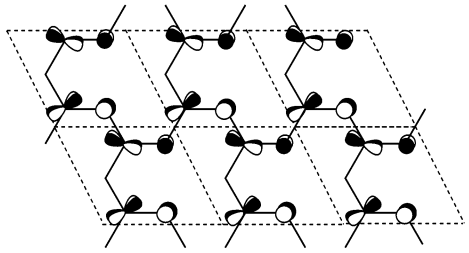

3

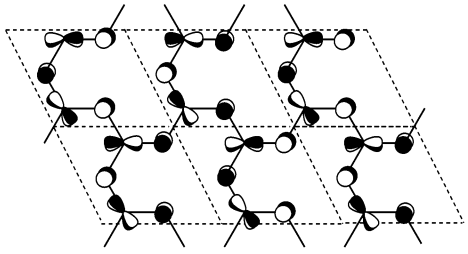

4

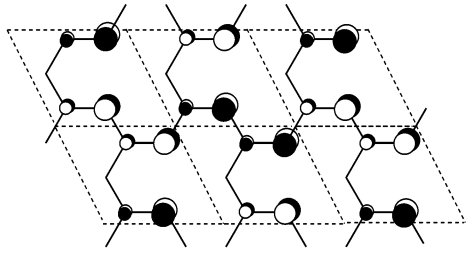

5

Finally, the lowest π level is primarily localized on Sn and is, of course, fully bonding between Sn and Ag at Γ. The behavior of the π bands is similar to those observed in graphite, or even more closely matches those in BN where the electronegativity difference between the two elements is similar to that between Ag and Sn. This relationship becomes clearer upon realization that the $[Ag_2Sn_3]^{-6}$ layer can be viewed as a defect graphite structure where every third Ag atom is missing. A hypothetical graphitic $[Ag_3Sn_3]^{-9}$ layer is the parent layer topologically and electronically analogous to BN.[69−71] For comparison, the band structure of the two-dimensional graphitic network, $[Ag_3Sn_3]^{-9}$, is shown on the left side of Figure 6. Its similarity to the band structure of BN is striking.[70,71] In both cases two filled σ bands lie above the three π bands at Γ. Above the filled bands are three empty π^* bands. Unlike graphite, but similar to BN, $[Ag_3Sn_3]^{-9}$ is predicted to be an insulator with a sizable, 2.1 eV gap, between filled and empty states. The addition of Ag atoms in going from $[Ag_2Sn_3]^{-6}$ to $[Ag_3Sn_3]^{-9}$ actually causes the two degenerate π orbitals at Γ to rise in energy, from −7.20 to −6.72 eV. The reason behind this is symmetry based. Referring back to **2** and **3**, only Ag d_{xz} and d_{yz} AO's can mix into these two crystal orbitals when the Ag atom is added at the center of each hetero[12]-annulene unit.[63] Since the Ag d orbitals lie at low energy, they will mix into **2** and **3** in an antibonding fashion destabilizing the π bands at the Γ point.

A similar, albeit more complicated pattern emerges for the highest lying σ orbitals. The shapes of the degenerate pairs of crystal orbitals, primarily of Sn p character, at Γ are represented by **6** and **7**. The Ag $d_{(x2-y2/xy)}$ set mixes into **6** and 7 in an

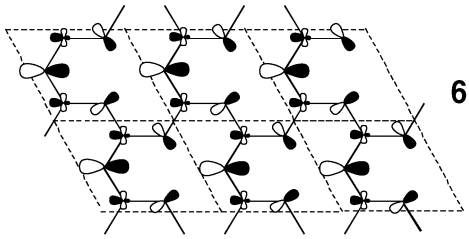

6

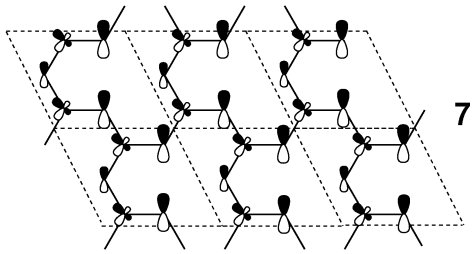

7

antibonding manner, but more importantly the Ag $p_{(x,y)}$ set mixes in a bonding manner. Therefore, the energies of the highest lying σ crystal orbitals do not significantly change in going from $[Ag_2Sn_3]^{6-}$ to $[Ag_3Sn_3]^{9-}$, i.e., the energies of the crystal orbitals at Γ are −5.29 and −5.33 eV, respectively. The bands for $[Ag_2Sn_3]^{-6}$ at lower energy are comprised of the three π orbitals previously mentioned. At still lower energies are the remaining

(69) Zupan, J. *Phys. Rev. B* **1972**, *6*, 6, 2477.
(70) Wentzkcowitch, R. M.; Chang, K. J., Cohen, M. L. *Phys. Rev. B* **1986**, *34*, 2, 1071.
(71) Burdett, J. K. *Chemical Bonding in Solids*; Oxford University Press: New York, 1995, 69.

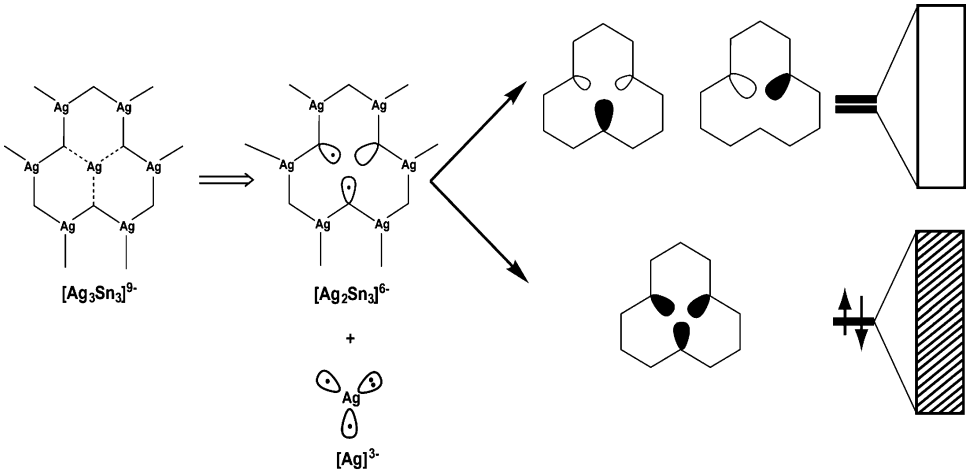

Figure 7. A simplified representation of the in-plane lone pairs in $[Ag_2Sn_3].^{6-}$ The three Sn sp^2 lone pair combinations produce *a1* and *e* combinations. These spread out into two bands, and the lower band *a1* is fully occupied.

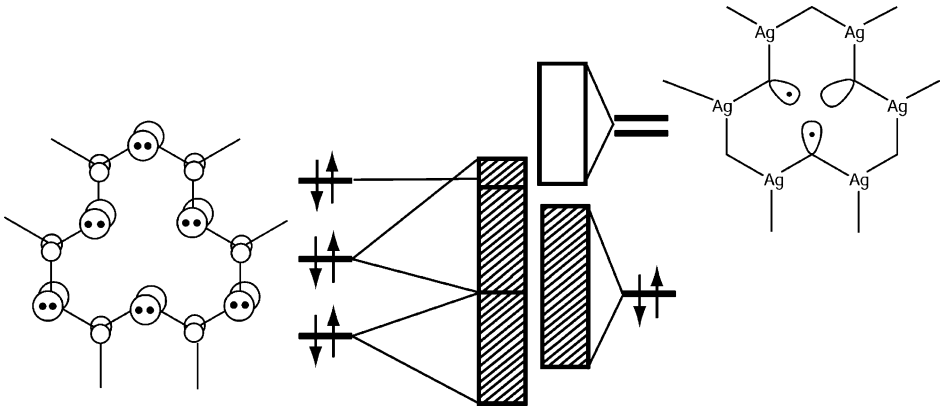

Figure 8. Diagramatic representation of the bands in $[Ag_2Sn_3].^{6-}$ On the left side are the three filled π orbitals, two of which have considerable dispersion. On the right side are the three in-plane hybrid orbitals which make up the trefoil state. The lowest combination is filled while the *e* set is empty.

σ orbitals that become progressively Ag d in character. However, there is one crystal orbital at Γ point, which consists almost solely of s-p hybrids at Sn as it is shown in **8**. The orbital lies at -8.91 eV and is accidentally degenerate with the lowest π band at Γ. The presence of this band offers a somewhat different perspective in viewing the electronic structure of this material.

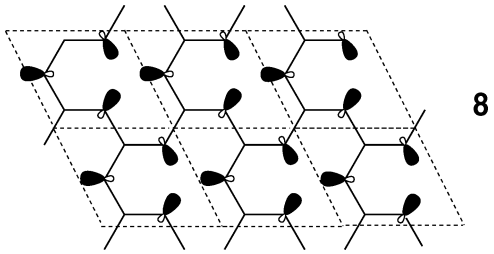

8

Consider the electronically "saturated" $[Ag_3Sn_3]^{-9}$ structure where all bonding and nonbonding bands are filled. For simplicity, let us also consider the d AO's at Ag to be completely filled and core-like, i.e., their involvement in bonding to Sn will be neglected. Each Ag and Sn atom then on the left side of Figure 7 can be viewed as having sp^2 hybridization in the σ framework. Removal of one central $[Ag]^{3-}$ atom then generates the $[Ag_2Sn_3]^{-6}$ unit. There are now three sp^2 hybrids at Sn that point toward the defect site and there are two electrons associated with these three hybrids. Linear combinations of the three sp^2 hybrids produce one totally in-phase combination and a pair of degenerate *e* set. The totally bonding combination is filled while in a formal sense the *e* set is empty. Coupling of these hybrid centers by AO's at Ag lead to bands with significant dispersion. A clear and direct relationship exists between the in-phase combinations of lone pairs (on the right-hand side of Figure 7) to **8**, as well as, between the *e* set to **6** and 7.

However, the real situation is a little more complicated than this. It would seem from the band structure plot (on the right-hand side of Figure 6) that a narrow gap is anticipated between the empty *e* set derived from the hybrids (illustrated on the right side of Figure 7) and the filled π bands. In fact the actual situation is schematically depicted in Figure 8. Consider the π system of the $[Ag_2Sn_3]^{-6}$ net as being constructed, as shown on the left side of Figure 8, from a "pentadienyl" $[Ag_2Sn_3]^{-6}$ unit that possesses only p AO's. With the assigned electron count there are then three filled π orbitals. The lowest two π orbitals have significant dispersion because of intercell overlap. However, higher lying HOMO for this system has no coefficient on Ag (neglecting the d AO's) and purely Sn based. Consequently, intercell overlap is negligible, and the band is expected to have no dispersion. This is illustrated in **9**−**11** for the **X** ($\mathbf{k}_x$=

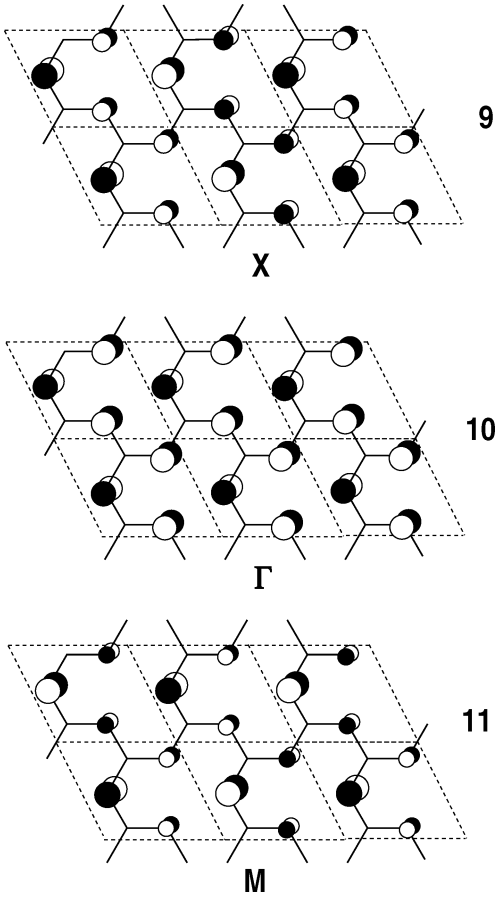

$\pi/\mathbf{a}$; $\mathbf{k}_y = 0$), Γ, and **K** points, respectively. Notice also in **9**−**11** that only d AO's on Ag have the correct symmetry to interact with the p AO combinations on Sn. This is also truefor the **X**, Γ, and **K** points; hence the inclusion of d AO's at Ag does not create any band dispersion. The superposition of the three Sn lone pair bands with the three π bands then leads to allowed band crossings and the resultant picture in the middle of Figure 8. The top of the filled π bands is partially emptied into the bottom of the bands derived from the Sn lone pair *e* set. The compound is, therefore, expected to be metallic and supported by resistivity measurements. Transport measurements on the title compound, using the Q-method,[56,57] show good metallic behavior as evidenced by the low resistivities and positive temperature dependence of the resistivity (Figure 9) over the temperature range of 100−295 K. The expected metallic behavior is also supported by the magnetic susceptibility measurements that indicate temperature independent paramagnetism (Pauli paramagnetism) over the temperature range 4−300 K. Furthermore, no magnetic transitions were observed for $Li_{17}Ag_3Sn_6$ down to 4 K.

The optimal bonding of the partially filled "lone-pair" sp^2 hybrids and the filling of the π-bands represents a stabilized "trefoil aromatic" state that was postulated about 20 years ago by Simmons and co-workers for a new class of aromatic molecules (e.g., annulenes and heteroannulenes).[72] Trefoil aromatics were said to possess a three-center two-electron bond (trefoil bond) that is imbedded in the center of an annulene perimeter containing $4n + 2$ π electrons. Fukunaga and

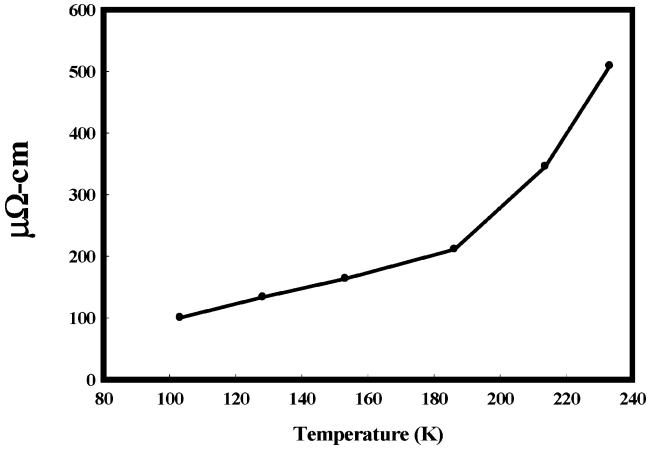

Figure 9. Temperature-dependent electrical resistivity behavior of $Li_{17}Ag_3Sn_6$.

Simmons proposed the stabilization of trefoilenes and heterotrefoilenes derived from their analogous annulenes and heteroannulenes.[72] In particular, they proposed the stabilization of a [6.6.6]trefoilene derived from a 12-annulene structure similar to the 12-membered ring of the $[Ag_2Sn_3]$ layer. However, molecular trefoil aromatics, proposed among annulenes and heteroannulenes, have not yet been observed. The trefoil aromaticity, postulated for aromatic molecular systems, is formally satisfied by the electronic structure of the $[Ag_2Sn_3]^{6-}$ layer in that the trefoil bonds (3-center, 2-electron) are optimized and the three π-bands are filled.

Naively from the bonding picture in Figure 7, one might expect significant Sn−Sn interaction exists between the three Sn atoms comprising this "trefoil" bonding arrangement[72] even though the Sn−Sn distance is significantly large − 4.41 Å. However, the partial occupation of the Sn lone pair *e* set, as indicated by Figure 8, will decrease the Sn−Sn bonding greatly. In our calculations the Sn−Sn overlap population was computed to be 0.015. It is significant that this value is a positive number despite the large interatomic distance. Adding more electrons per unit cell to totally fill the Sn lone pair *e* set and nonbonding π band decreases the Sn−Sn overlap population to −0.077.

Three-dimensional calculations on the complete anionic structure, $[Ag_3Sn_6]^{17-}$, confirm the electronic structure analyses based on $[AgSn_3]$ and $[Ag_2Sn_3]$ layers. The calculated three-dimensional band structure is essentially a superposition of the rigid band structures of the $[AgSn_3]$ and $[Ag_2Sn_3]$ layers. The placement of the Fermi level also confirms the electron allocations of $[AgSn_3]^{11-}$ and $[Ag_2Sn_3]^{6-}$. Thereby the occupied electronic states associated with the Zintl layer, composed of CO_3^{2-}-like $[AgSn_3]^{11-}$ anions, lie deep below the Fermi level. While the electronic states of the trefoil-stabilized $[Ag_2Sn_3]^{6-}$ π network dominate the states around the Fermi level and the conduction band, and these states greatly influence the electronic properties of the polar intermetallic.

To assess the contributions of lithium electronic states to the chemical bonding of $Li_{17}Ag_3Sn_6$, more spophisticated LMTO-ASA calculations were performed.[73] This is also in relation to the ability of lithium to stabilize peculiar anionic substructures with high formal charges. Results of the calculation indicate

(72) Fukunaga T.; Simmons H. E.; Wendoloski J. J.; Gordon M. D. *J. Am. Chem. Soc.* **1983**, *105*, 2729.

(73) Jepsen, O.; Andersen, O. K. *STUTTGART TB-LMTO-ASA Program*; Max-Planck-Institut für Festkörperforschung: Stuttgart, 2000.

significant mixing of Li states with the occupied valence states and similar interactions of the $AgSn_3$ and Ag_2Sn_3 substructures with Li. These can be attributed to the similar lithium coordination of the anion fragments. Also, as in the previous semiempirical calculations, the d-states of Ag are localized and lie well below the Fermi level. Orbital analyses of the σ and π interactions within the anionic fragments confirm the extended-Huckel results, validating the carbonate-like description of the $AgSn_3$ fragments and the overall trefoil bonding description of the Ag_2Sn_3 network. However, the mixing of the lithium states with the two AgSn fragments, $AgSn_3$ and Ag_2Sn_3, indicates that these electronic entities are not completely isolated but are significantly influenced by their surrounding Li neighbors. These important lithium interactions provide an effective way of stabilizing the high formal charges on the $[AgSn_3]^{11-}$ and $[Ag_2Sn_3]^{6-}$ anion substructures.

The bonding picture of the $[Ag_2Sn_3]^{6-}$ layers described here is in contrast to that for Yb_3Si_5.[65,66] As mentioned earlier, the Yb_3Si_5 compound features a two-dimensional hexagonal network of Si atoms, like graphite, where every sixth Si atom has been removed. If a simple ionic description of the bonding is invoked and a closed-shell $4f^{14}$ configuration is considered for Yb then the structure can be viewed as $[3\ Yb^{2+}]\ [Si_5^{6-}]$. One might expect that the Si_5^{6-} structure would lead to a complete filling of the Si lone pairs analogous to those shown in Figure 7 for Sn. Of the five π bands in the Si_5^{6-} unit cell, four will be filled. Following the classical Zintl approach, Pottgen and coworkers assigned the Si_5 network as Si_5^{8-}.[66] The Si_5^{8-} electronic assignment would be analogous to a saturated unit where all lone pair states are completely occupied. The 8 electronic charges on the Si network are obtained from the Yb atoms ($2Yb^{3+}$ and $1Yb^{2+}$), also resulting in a mixed-valent assignment of the rare earth metal atoms.[66] However, the geometry of the Si layer is deformed as shown in **12**. The Si−Si−Si angles that

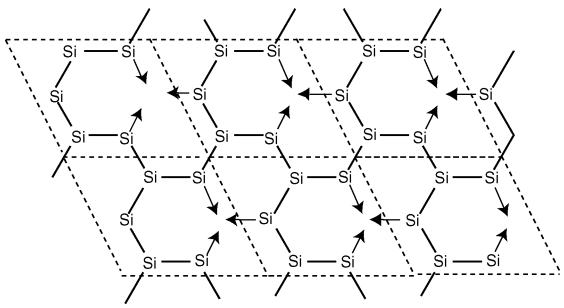

12

form the inner core of the [12]-annulene unit decrease from 114.83° as observed in our structure for the Ag−Sn−Ag angle of the $[Ag_2Sn_3]^{6-}$ layer to 102°. The angular deformation around the vacant sites of the Si_5 network causes the *e* set of the lone pairs (see Figure 7) to rise considerably higher in energy. In fact, an extended Hückel calculation on Si_5^{6-} shows that the five π bands are totally filled and the Si lone pair *e* set is one-half occupied. The nonbonded (representing the Si in-plane lone-pair interaction) Si−Si overlap population for this electron count is computed to be 0.017 (the Si−Si distance is 3.00 Å as opposed to the Si−Si distance of 2.42 Å for the directly bonded Si atoms). Adding two more electrons per unit cell (Si_5^{8-}) completely fills the lone pair orbitals, and the corresponding Si−Si overlap population becomes −0.326. Pöttgen and coworkers also carried out extended Hückel calculations on Yb_3Si_5 that included Yb atoms and found that significant bonding exists between Yb and Si.[66] Furthermore, their calculations indicate electron density from the Fermi level of the Si_5^{6-} layer is actually removed so the electron density from Si lone pair *e* set is further reduced which increases the Si···Si bonding. In their computations the nonbonded Si···Si overlap population was in fact found to be 0.152. One may rationalize the seemingly opposing effects of the electronic structure and deformation of the Si_5 network (shown in **12)** of Yb_3Si_5 in terms of increased covalency of the Yb−Si interactions and the matrix effects of the larger Yb atoms. Increased covalency would nominally decrease the electron count on the Si_5^{6-} network thereby increasing the Si···Si bonds across the vacancies. Also, the Yb atoms in Yb_3Si_5 are located directly above and below the centers of the nominal hexagons of the Si_5 network. Matrix effects of the larger Yb atoms will tend to deform the Si network to offset the vacancies of the Si_5 layers. This is further enhanced by increased Yb−Si bonding. In $Li_{17}Ag_3Sn_6$, matrix effects by Li on Ag and Sn are negligible and the different location of Li atoms above and below the vacancies aid in stabilizing the defects within the $[Ag_2Sn_3]^{6-}$ trefoil network.

Conclusion

The rich structural diversity exhibited by late-transition metal polar intermetallics has revealed a remarkable success of the Zintl concept in rationalizing their synthesis, structure, and chemical bonding. Although there remain unresolved questions about the physical accuracy of the Zintl picture, it can be effectively used as a rational approach in designing and rationalizing new complex layered transition metal polar intermetallics. The newly discovered polar intermetallic compound, $Li_{17}Ag_3Sn_6$, illustrates this point. The complex late transition metal polar intermetallic exhibits a unique and complex structure type that features an anionic substructure derived from the intergrowth of graphite-like and Kagome nets. The structure features slabs of $Li_{10}[AgSn_3]$, with isolated $[AgSn_3]^{11-}$ anions, alternately stacked with $Li_7[Ag_2Sn_3]$ slabs, having $[Ag_2Sn_3]^{6-}$ defect-honeycomb nets. Extended Hückel band structure calculations indicate that the seeming electron deficiency of the polar intermetallic, with respect to the classical Zintl definition, is accommodated by unique metallic bonding schemes associated with aromatic and unsaturated hydrocarbons. Band structure calculations further show that the chemical bonding in $Li_{17}Ag_3Sn_6$ is effectively optimized. The $[AgSn_3]^{11-}$ anions are described as being isoelectronic and analogous with the CO_3^{2-} anion. More interestingly, the $[Ag_2Sn_3]^{6-}$ layers are found to exhibit significant π-bonding interactions such as BN and graphite. In addition the chemical bonding of the unique anionic layer is further optimized through the formation of a "trefoil" bonding state (σ-aromaticity) previously proposed for molecular systems, and finally encountered in an extended intermetallic network. This emphasizes the surprising yet crucial role of interactions among incompletely filled lone-pair orbitals in the stabilization of layered intermetallic anion structures. This work also clearly illustrates the importance of the nature of the cations (size, charge, moles, electronegativity), electronegativity differences of the transition and posttransition metals of the anionic substructure, electronic factors (electron counts and lone pair interactions), and matrix effects in the structural preferences of

transition metal polar intermetallics. Interplay of these crucial factors lead to important structural adaptations and deformations.

Since unique structures and properties are already apparent in classical Zintl phases, it is anticipated that exploratory studies on late transition-metal polar intermetallics, along the Zintl border, will lead to the discovery of not only unusual crystal chemistry but unique chemical bonding and interesting electronic properties as well. These studies will significantly improve our understanding of intermetallic compounds (establishing structure-bonding-property relationships) beyond the Zintl border.

Acknowledgment. The authors would like to thank Prof. J. D. Corbett for providing the Q-measurements, and Prof. U. Häussermann for helpful comments regarding the LMTO-ASA calculations. Financial support for this work is provided by the National Science Foundation (CAREER Award, DMR-9733587), the Texas Center for Superconductivity and Advanced Materials at the University of Houston, the Petroleum Research Fund administered by the ACS, and the R.A. Welch Foundation. This work made use of MRSEC/TCSUH Shared Experimental Facilities supported by the NSF (DMR-9632667) and the State of Texas through the TCSUH.

Supporting Information Available: Crystallography tables and X-ray crystallographic files in CIF format for the structure determination of $Li_{17}Ag_3Sn_6$; DOS plots (PDF). This material is available free of charge via the Internet at http://pubs.acs.org.

JA038868N